Studies of ^{3}He confined to a submicron slab geometry

Second Year Report

Antonio Córcoles

September 2003- August2004

Supervisor: Professor J. Saunders

Advisor: Dr. F. M. Grosche

Moderator: Dr. G. C. Cowan

Contents

List of Figures

1 Brief summary of the year

As stated in last year's report and regarding the promising results from the NMR experiment, the idea from early October, after attending two summer schools in Ambleside and Helsinki, was to carry on with those measurements, get deeper insight in the evolution of the several NMR peaks observed and investigate further the morphology of the sample by playing around with the magnet gradients. Unfortunately, the SQUID died at the beginning of September. The feedback coil was found shorted to the SQUID. This event changed the whole schedule, since we needed to get another NMR probe ready. This has been one of the main activities of the year together with the Torsional Oscillator experiment. Complementary activities have been leak testing a sample of optical bonding and a theoretical treatment of the capillary condensation of the ^{3}He in our cell. I have attended, in addition, the Low Temperature Techniques IOP course in Birmingham in November 2003 and the International Symposium QFS 2004 holded at Trento, Italy, between the 4^{th} and the 11^{th} of July of the present year.

2 Invitation: a little of theory

2.1 In the beginning it was ^{3}He

^{3}He is, undoubtedly, one of the richest systems to do experimental physics with. Not only is it the more complex material we can approach with the support of a successful theory, but also it has a wide and unexplored field behind it as well as connections with almost any branch of modern theoretical physics.

Shortly after the formulation of the BCS theory in 1957 by Bardeen, Cooper and Schrieffer [1], the question arised of whether such a mechanism would take place in ^{3}He. Due to the strong short-distance repulsion between the ^{3}He atoms, the l=0 component of the quasiparticle interaction becomes repulsive and cannot lead to any pairing. A number of higher orbital angular momentum pairing states were proposed then, giving special attention to the p-wave (l=1) and d-wave (l=2) candidates. Whereas the l=2 state was at first considered the most favorable [2], the l=1 state, which implied total spin s=1 due to Pauli's exclusion principle, turned out to be the actual solution for the superfluid state of ^{3}He. The p-wave state was first studied in detail by Balian and Werthamer [3] in 1963 when they were concerned about the spin susceptibility of superconductors in a s=1 state.

Superfluid ^{3}He was finally first observed by Osheroff, Richardson and Lee in 1971 [4] while doing Pomeranchuk cooling. They observed two anomalies, which they called A and B, in the melting pressure of their Pomeranchuk cell as the cell volume was changed at a constant rate. Both features were observed in cooling and warming, with the kink at B (at around 2.1 mK) being different in both cases and history dependent. That suggested a first order phase transition in the B signature. The A characteristic was observed

always at the same pressure (corresponding to a temperature of about 2.7 mK in the melting curve). It was thought that the A anomaly corresponded to a second order phase transition. Several NMR experiments performed by the same group at Cornell [5] gave very interesting results. Firstly, a NMR frequency shift was observed in the A transition and the shift increased as the temperature decreased. In the B transition, on the other hand, there was not such a shift, but the susceptibility decreased slowly below the B point and only a small amount. The fact that the magnetic susceptibility did not approach zero was a confirmation of a pairing state other than s=0. That meant that l could not be an even number and, therefore, the l=1 pairing state was the most probable candidate. The first successful reconciliation of the novel results with the BCS picture came from Leggett [6], who not only explained correctly the NMR shifts observed, but also predicted a longitudinal resonance observed later.

In order to sketch the theory behind superfluidity in ^{3}He, we can take two approaches. First, we could try to understand it from a macroscopic and phenomenological point of view such as the Landau-Ginzburg theory of continuous phase transitions [7] [8]. Another alternative would be to describe the microscopic behavior of the system using the BCS [1] theory. Gorkov was, in 1959, [9] able to derive the Landau model from the BCS theory.

2.2 The BCS side of the story

The core of the BCS theory of superconductivity states that two identical Fermi particles with momentum $\hbar k$ and $\hbar k'$ near the Fermi surface and in the presence of a filled Fermi sea, can interact through some potential in such a way that the total energy of the final state for these two particles

would be less than twice the Fermi energy. In other words, they can form a bound state, the so-called **Cooper pair**. The potential used by Bardeen *et. al.* to compute the ground state was the following:

$$V_{\mathbf{kk'}} = \begin{cases} -V & \text{for } k_F - \Delta k \leq k, k' \leq k_F + \Delta k, \\ 0 & \text{otherwise} \end{cases} \tag{1}$$

where $\Delta k \ll k_F$ is assumed. The interaction, thus, can only affect particles within a narrow shell near the Fermi surface and this is because the Pauli principle prevents the particles well inside the Fermi sphere to scatter into other levels since they are all occupied. The other fundamental ingredient apart from (1) is the assumption that the Fermi surface is spherical in shape. Now, we construct the system wave function not referring to *pair of particles*, but to *pairs of single-particle states* ($\mathbf{k}\uparrow, -\mathbf{k}\downarrow$) corresponding to spin singlet pairing. At zero temperature, i.e. the ground state, each state ($\mathbf{k}\uparrow, -\mathbf{k}\downarrow$) is either full or empty. With $|0,0>$ we will mean that the pair is unoccupied and with $|1,1>$ that it is occupied. Thus, we have the wave function

$$\Phi = \prod_k \Psi_k \tag{2}$$

where

$$\Psi_k = u_k^* |0,0> + v_k |1,1> \tag{3}$$

$|u_k|^2$ is the probability that the pair ($\mathbf{k}\uparrow, -\mathbf{k}\downarrow$)is unoccupied and $|v_k|^2$ is the probability that it is occupied Obviously, at T=0,

$$u_k = 0 \quad \text{and} \quad v_k = 1 \quad \text{for} \quad |\mathbf{k}| < k_F$$

$$u_k = 1 \quad \text{and} \quad v_k = 0 \quad \text{for} \quad |\mathbf{k}| > k_F$$

and normalisation requires

$$|u_k|^2 + |v_k|^2 = 1$$

We will now use a variational method to calculate the solutions of the system under study. To do that we first need an expression for the mean value of the Hamiltonian. The kinetic energy is easy, simply

$$< \Phi|K - \mu N|\Phi >= \sum_k 2\epsilon_k |v_k|^2 \tag{4}$$

where K is the kinetic energy operator, N is the number of particles, μ is the chemical potential and ϵ_k is the energy of *one* particle (therefore the factor 2). The term μN is a constriction introduced due to the fact that we are not working under a constant number of particles. The reason for this is that the number of particles and the phase of the wave function are *conjugate* variables and therefore there exists an uncertainty relationship. Now we account for the potential part of the Hamiltonian. The required expression is:

$$< \Phi|V|\Phi >= \sum_{k,k'} V_{k,k'} u_k v^*_{k'} u^*_{k'} v_k \tag{5}$$

because when the pair ($\mathbf{k}\uparrow, -\mathbf{k}\downarrow$) scatters into (**k'** $\uparrow, -$**k'** $\downarrow$), not only the state ($\mathbf{k}\uparrow, -\mathbf{k}\downarrow$) has to be initially full (probability v_k) but also the state (**k'** $\uparrow, -$**k'** $\downarrow$) has to be empty (probability $u^*_{k'}$). The next step is to minimize the complete expectation value with respect to variations in the occupation probabilities. Defining

$$\Delta_k = \sum_{k'} V_{k,k'} u_{k'} v_{k'} \tag{6}$$

we obtain after some algebra the well-known expression for the ground state BCS energy gap:

$$\Delta_k = -\sum_{k'} V_{k,k'} \frac{\Delta_{k'}}{2E_{k'}} \tag{7}$$

where $E_k^2 = \epsilon_k^2 + |\Delta_k|^2$

If we want to extend the present treatment to finite temperatures, we must allow some other states into the wave function, namely, the "broken pair" states $|1,0>$ and $|0,1>$ (which account for $(\mathbf{k}\uparrow)$ occupied and $(-\mathbf{k}\downarrow)$ unoccupied, etc.). The calculations are straightforward and the general expression for the BCS gap equation is obtained:

$$\Delta_k = -\sum_{k'} V_{k,k'} \frac{\Delta_{k'}}{2E_{k'}} tanh \frac{E_{k'}}{2k_B T} \tag{8}$$

In view of this result, let us point out that the gap equation defines only an extremum of the free energy. In the case of superconductors this is not a problem since there is only one extremum which is also a minimum. But for $l \neq 0$ the gap equation provides several solutions, some of them not even an extremum but a saddle point. The energy E_k can be shown to be the energy of an elementary excitation [6].

This much for information in superconductors. Then, what happens when the pairing occurs in a wave higher than zero, like in superfluid ^{3}He? In an incredibly short period of few weeks, Anthony Leggett [6] extended the BCS treatment of superconductivity to superfluid ^{3}He, not only thus explaining the enormous amount of data constantly coming out the top research laboratories around the world, but also predicting new features, like the longitudinal NMR ringing, later confirmed. The effective interaction in liquid ^{3}He is rather complicated due to the extension of the hard-core repulsion potential, which is comparable with the interatomic distance. We

need, therefore, to describe the liquid in terms of Landau "quasiparticles" rather than real atoms. We have said previously that the pairing in superfluid ^{3}He occurs in p-wave. This kind of pairing implies a total spin $s = 1$ due to the fermionic nature of the ^{3}He quasiparticles (the wave function must be antisymmetric). The spin subspaces are then $|\uparrow\uparrow>$, $|\downarrow\downarrow>$ and $|\uparrow\downarrow + \downarrow\uparrow>$. Whereas for the $l = 0$ case we had a wave function of the form

$$\Psi(k) = \Psi_{\uparrow\downarrow}(k)(|\uparrow\downarrow - \downarrow\uparrow>) \tag{9}$$

we have to write now

$$\Psi(k) = \Psi_{\uparrow\uparrow}(k)|\uparrow\uparrow> + \Psi_{\downarrow\downarrow}(k)|\downarrow\downarrow> + \Psi_{\uparrow\downarrow}(k)(|\uparrow\downarrow + \downarrow\uparrow>) \tag{10}$$

(These wave functions are not normalised). Now, of course, the BCS gap could have different values for different spin subspaces. We have to define

$$\Delta(k) = \begin{pmatrix} \Psi_{\uparrow\uparrow}(k) & \Psi_{\uparrow\downarrow}(k) \\ \Psi_{\downarrow\uparrow}(k) & \Psi_{\downarrow\downarrow}(k) \end{pmatrix} \tag{11}$$

Each of the above matrix elements follows (8). This is not, however, the most convenient way to express the pairing. We can introduce [3] a vector representation with Leggett notation

$$\mathbf{d}(k) = \frac{1}{2} \quad i\sum_{\alpha\beta}(\sigma_y \boldsymbol{\sigma})_{\alpha\beta}\Psi_{\alpha\beta}(k) \tag{12}$$

where σ's are the Pauli matrices and the subindexes run over the spin states $\uparrow$ and $\downarrow$. Then, turning things around, we get

$$\Delta(k) = \begin{pmatrix} -d_x(k) + id_y(k) & d_z(k) \\ d_z(k) & d_x(k) + id_y(k) \end{pmatrix} \tag{13}$$

In order to physically interpret further the meaning of the **d** vector we could calculate the value of the square of the gap, i.e. $\Delta\Delta^+$.

$$\Delta\Delta^+ = (d \cdot d^*)I + i\sigma \cdot (d \times d^*) \tag{14}$$

We now define an **unitary state** as one for which $\Delta\Delta^+$ is proportional to the unit matrix. That implies $\mathbf{d} \times \mathbf{d}^* = \mathbf{0}$ for an unitary state or, in other words, **d** is a real vector and the excitation energy E_k is a number rather than a matrix. It can also be shown [11] that $\mathbf{d} \cdot \mathbf{S} = 0$, so the modulus of **d** tells us the magnitude of the gap for an unitary state and its direction is the direction of zero spin projection. One more character should appear on the scene, finally. If we express the **d** vector as a function of the **k** vector,

$$d_i(k) = \sum_\rho A_{i\rho} k_\rho \tag{15}$$

we obtain a 3×3 complex matrix $A_{i\rho}$ and whereas in the case of superconductors we had only two degrees of freedom (the amplitude and the phase of the wave function), we have now 18 degrees of freedom from the A matrix. Fortunately, they are not all independent in the stable phases, so we will not need to deal with intractable systems. The A matrix is absolutely equivalent to the **d** vector when describing the pairing in superfluid ^{3}He.
With all the information we gathered so far, we can talk briefly about the observed experimental superfluid phases of ^{3}He.

2.2.1 *B phase*

The B phase is the stable phase at low pressures and in absence of magnetic field (the so-called weak coupling limit). This phase has an isotropic energy gap, but intrinsically, it is not at all isotropic. In fact, ^{3}He is an anisotropic superfluid in all its phases. The B phase is anisotropic in the following sense: in the most general state, the **d** vector, which points radially away from the center of the Fermi sphere, is rotated about an arbitrary axis, which we will call N, by an angle ϕ. So the magnetic dipolar energy varies all over the Fermi surface and it depends on the angle ϕ. The A matrix for the B phase is

$$A = \Delta \begin{pmatrix} 1 & 0 & 0 \\ 0 & 1 & 0 \\ 0 & 0 & 1 \end{pmatrix} \tag{16}$$

This phase is described by the Balian and Werthamer state [3] and its magnetic susceptibility is reduced with respect to the normal Fermi fluid due to the $|\uparrow\downarrow + \downarrow\uparrow>$ part of the pairing (the B phase contains all three of the possible spin substates).

2.2.2 *A phase*

The A phase needs some 30 bar of pressure to become stable. It can also be more favourable energetically than the B phase in a magnetic field or in a state of confinement. The stabilisation mechanism for the A phase pairing is called *spin fluctuation feedback* and it is due to the very formation of the condensate. In the case of ^{3}He there is no lattice with which the

quasiparticles interact and the onset of superfluidity changes the pairing interaction. The idea of spin fluctuation feedback was first introduced by Anderson and Brinkman [12]. Its pairing states are only Equal Spin Pairing (EPS) states, that is, $|\uparrow\uparrow>$ and $|\downarrow\downarrow>$, so its magnetic susceptibility is the same as for the normal Fermi liquid. The **d** vector for the A phase has the form of the Anderson-Brinkman-Morel state (ABM), which is

$$d(k) = \sqrt{3/2} \quad \Delta \quad (k_1 + ik_2) = \sqrt{3/2} \quad \Delta \quad |k| \sin\theta e^{i\phi} \tag{17}$$

and thus

$$\mathbf{d} \cdot \mathbf{d}^* = |(d(k))|^2 = 3/2\Delta^2 \sin^2\theta \tag{18}$$

so the energy gap has two nodes in k space in the k_z direction and the vector **d** points in the same direction in spin space for all points on the Fermi sphere. The form of the A matrix in the ABM state is:

$$A = \Delta \begin{pmatrix} 1 & i & 0 \\ 0 & 0 & 0 \\ 0 & 0 & 0 \end{pmatrix} \tag{19}$$

Let us remark that in an applied magnetic field, the A phase is no longer an unitary state, since the components $\Psi_{\uparrow\uparrow}$ and $\Psi_{\downarrow\downarrow}$ are not equal in this case which implies that $\Delta\Delta^+$ is not an unitary matrix. This leads to a different phase, called A_1 in which only one spin population is present.

2.2.3 *Planar phase*

If we would confine the ^{3}He in some restricted geometry, the size effects would of course affect the A matrix. If we assume, without lost of generality, that the sample lies in the x-y plane, then the z component of the **d** vector

would be suppressed, leading to the following A matrix:

$$A = \Delta \begin{pmatrix} 1 & 0 & 0 \\ 0 & 1 & 0 \\ 0 & 0 & 0 \end{pmatrix} \tag{20}$$

This occurs due to the suppression of the $\Psi_{\uparrow\downarrow}(k)$ part of the wave function, so the planar phase resembles the character of the A phase although the A matrix could, at first sight, suggest a similarity with the B phase. It also has, as the A phase, two nodes along the k_z axis. The difference with the A phase is that the remaining spin states have opposite angular momentum eigenvalues, so there is not a net orbital angular momentum for the planar phase.

2.3 The Ginzburg-Landau approach

The Landau theory of continuous phase transitions applies to changes in a system from a disordered state to an ordered state. A good example of this could be the transition between paramagnetism and ferromagnetism at the Curie point in magnetic materials, the Bose-Einstein condensation and, of course, the superfluid and superconducting transitions. The continuous phase transitions, also known as Second Order phase transitions, have no associated latent heat. They rather imply a change in the symmetry of the system. The word *continuous* refers to the fact that the *energy* changes continuously, although the symmetry changes discontinuously. The symmetric elements in a body are either present or absent, and therefore it is meaningless to think about a *continuous symmetry change*. The Ginzburg-Landau theory states that we can describe a continuous transition by an "order parameter", that is, some quantity which is zero or very small

above the transition and rises as we go into the ordered phase. In the previous examples, we could use the magnetic susceptibility in the Curie transition, the condensate density in the Bose-Einstein condensation and the A matrix described above in the superfluid transition. After defining an order parameter, the next step is to express the free energy as a function of that order parameter and minimize it. To a low order approximation, we can write down the free energy as a function of the order parameter as follows:

$$F = -\alpha|A|^2 + \beta|A|^4 + K|\nabla A|^2 \tag{21}$$

where the last term accounts for spacial changes on the order parameter. This order parameter only appears in even powers due to symmetry reasons (an easy, although not too rigorous argument would be that the free energy is a scalar quantity whereas the order parameter is a tensor in its more general form). Let us momentarily forget about the spacial variations of the order parameter. If we minimize the free energy with respect to the order parameter we find that $A = \sqrt{\alpha/2\beta}$ and $\alpha \sim (T - T_c)$ since it has to be zero at the transition point. If we now regard the order parameter as a 3×3 complex matrix (case of superfluid ^{3}He) we can express the free energy in the following way:

$$F = -\alpha(T)A^*_{i\mu}A_{i\mu} + \beta_1 A^*_{i\mu}A^*_{i\mu}A_{j\nu}A_{j\nu} + \beta_2 A^*_{i\mu}A_{i\mu}A^*_{j\nu}A_{j\nu} + \beta_3 A_{i\mu}A^*_{j\nu}A^*_{i\nu}A_{j\mu} + \\ + \beta_4 A_{i\mu}A^*_{i\nu}A_{j\nu}A^*_{j\mu} + \beta_5 A_{i\mu}A^*_{j\nu}A_{i\nu}A^*_{j\mu}$$

or

$$F = -\alpha(T)TrAA^{+} + \beta_1|TrAA^{T}|^2 + \beta_2(TrAA^{+})^2 + \beta_3 Tr(AA^{T})(AA^{T})^{*} + \\ + \beta_4 TrAA^{+}AA^{+} + \beta_5 Tr(AA^{+})(AA^{+})^{*} \quad (22)$$

where A^{+} is the hermitian conjugate and A^{T} is the transpose matrix. The free energy, being a scalar, has to be invariant under symmetry transformations. The Gauge symmetry implies a change in phase, so each term must have as many A's as A^{*}'s. Invariance under rotation in the real space (greek letters in the tensor notation) requires contracting the μ and ν indexes and similarly with the first index (latin letters). In the weak coupling limit (the limit in which the B phase is stable), the BCS theory predicts:

$$\alpha^{BCS}(T) = \frac{N(0)}{3}\Big(1 - \frac{T}{T_c}\Big) \quad (23)$$

$$\beta_1^{BCS} = -N(0)\Big(\frac{1}{\pi k_B T_c}\Big)^2 \frac{1}{30}\frac{7}{8} \quad \zeta(3) \quad (24)$$

and

$$-\beta_5^{BCS} = \beta_4^{BCS} = \beta_3^{BCS} = \beta_2^{BCS} = -2\beta_1^{BCS} \quad (25)$$

where $N(0) = k_F^3/(2\pi^2 v_F p_F)$ is the single spin quasiparticle density of states at the Fermi surface. In the strong coupling limit, where the A phase is stable, there are further corrections in β_i's. Now we are ready to take into account spatial variations of the order parameter. In the simpler case of superconductors (21) we could define a new variable $f = A/\sqrt{\alpha/2\beta}$ and reformulate the equation:

$$\frac{K}{\alpha}\frac{d^2 f}{dx^2} + f - f^3 = 0 \quad (26)$$

We now define a characteristic length $\xi_s = \sqrt{K/\alpha} = \sqrt{K/\alpha_0}(1 - T/T_c)^{-1/2}$ This length becomes infinite at T_c and can be regarded as the minimum length over which the wave function of the Cooper pair is allowed to vary, that is, the size of the Cooper pair. In the case of superfluid ^{3}He, Ambegaokar *et. al.* [13] wrote

$$F_{grad} = \sum_p \{K_L|\nabla \cdot A_{pi}|^2 + K_T|\nabla \times A_{pi}|^2\} \tag{27}$$

for the gradient contribution to the free energy. From the above expression we can deduce a transversal and longitudinal correlation lengths:

$$\xi_L^2 = \sqrt{K_L/\alpha} = \frac{9}{5} \quad \xi_s^2/(1 - T/T_c) \tag{28}$$

$$\xi_T^2 = \sqrt{K_T/\alpha} = \frac{3}{5} \quad \xi_s^2/(1 - T/T_c) \tag{29}$$

The correlation length of superfluid ^{3}He (ξ_s) is of the order of 65 nm at zero pressure and zero temperature.

2.4 The road towards 2D

In a confinement state, two possible phases in superfluid ^{3}He films are expected [15] [16] [17], one of which is A-like (Equal Spin Pairing) and the other is B-like. They are low-dimensional manifestations of the planar phase discussed above. The planar phase is a perfect 2D state whereas a film of ^{3}He in the real world is a 3D sample unless we would be studying a monolayer, which is not the case. When the system undergoes the superfluid transition, the confinement provides it with a two-dimensional nature due to the suppression of the order parameter. The only component of the A-like phase order parameter is referred to an orbital motion of the quasiparticles parallel

to the film surface. The B-like phase has both, parallel and perpendicular components [14]. At low pressures the A-like phase is first seen, instead the B phase that could be expected in bulk superfluid ^{3}He, and the reason is that the coherence length diverges at T_c so the only possible orbital motion is that in the plane of the film. That rules out the B-like phase. As the temperature decreases, so does the coherence length and a point is reached when the pair is allowed to move perpendicular to the film. This situation is similar to that in bulk and the B-like phase becomes more stable.

The boundary conditions strongly influences the behavior of the order parameter in the same way as a magnetic field does. For specular scattering there is no suppression in the amplitude of the order parameter, only its structure varies. The transverse components remain unaltered and the longitudinal component is strongly suppressed. This implies no suppression in the temperature of the Normal→A transition, but still a suppression in the temperature of the A→B transition. This is also the reason why the effective thickness of a film in contact with only one substrate and a free surface at zero pressure (which reflects specularly) is twice the real thickness as far as the A transition is concerned. For diffusive scattering all the components are affected and both transition temperatures are suppressed [18].

2.5 What is all this for? Present and future of the subject

The motivations for this research are countless. As mentioned in the introduction, ^{3}He is related with almost any other field in physics. Several areas of knowledge could be improved by this research. We will give some brief examples. The Kosterlitz-Thouless 2-D phase transition [19], first seen in ^{4}He films, has recently been observed in a d-wave superconductor [20] and ^{3}He films could be another system where it could be studied. An Ising-like

phase transition has been suggested by Stein and Cross [21]. The subject of layered superconductors could also be benefited from this research and, finally, since the confinement makes the quasiparticles behave more like "particles in a box", the Fermi surface could not be a sphere any more, but a set of "Fermi discs" (de Haas van Alphen effect) whose number could be tuned by the thickness of the film. This is analogous to the Quantum Hall effect.

2.5.1 Experiments done on superfluid ^{3}He in restricted geometries

Studying a more or less thin film of ^{3}He in a research laboratory is a remarkably challenging task from the technical point of view. The sample cannot spread over a large area if an uniform film thickness is desired and a small sample is difficult to detect. In this work we use two ultra-sensitive apparatii to observe our material: a tuned SQUID NMR system, capable of observing samples as small as 10^{17} atoms, developed by Helen Dyball [22] in her Ph. D. project and which is run in collaboration with PTB in Germany and a Torsional Oscillator developed in collaboration with J. Parpiak at Cornell University.

The first sight of film superfluidity in ^{3}He took place in 1985 at Queens University [23] when observing a self-emptying beaker. They reported a superfluid transition higher than that of bulk, which contradicted the predictions. This was later attributed to an error in the measurement of the temperature. The work was followed by a number of measurements and theoretical analyses by different groups. In another experiment at Berkeley [24], a stable saturated ^{3}He film was seen for the first time. That same year, 1988, another group at Cornell [25] performed an experiment

with the same techniques used in the present work, namely, NMR and the Torsional Oscillator. They studied a single effective film thickness with a stack of Mylar sheets evenly spaced (280 ± 20 nm.). One of their main contributions, apart from observing a clear suppression in T_c, was to study the effect of the scattering by adding a layer of ^{4}He to the substrate. Finally, in 1990 at Purdue University, Xu and Crooker [26] used a torsional oscillator consisting of a plate suspended over a bath of ^{3}He where they grew films of several thicknesses. The fact that the film thickness was not stable turned out to be an advantage, since they could study different thicknesses with each sample. Their films ranged from 83 to 172 nm and at temperatures down to 0.35 T_c. Since their films had a free surface, the effective thickness was actually twice the real thickness. When they plotted the data of the superfluid density vs. reduced film thickness ($d/\xi(T)$) they observed two completely different behaviors depending on whether the film was thicker or thinner than $1375\mathring{A}$. They could not, however, identify the observed superfluid phases.

There have been several theoretical calculations regarding the novel superfluid phases of ^{3}He. We should mention, apart from the above, the work by Li and Ho [27] and the work by Kjäldman *et. al.* [28].

3 The SQUID NMR Probe

By the middle of September, the SQUID placed on the cryostat showed a bizarre behavior. The IV characteristic did not show an horizontal region, but rather two straight lines with different slopes. The V-ϕ characteristic had, in turn, a decreasing trend. The diagnostic was that the feedback coil was shorted to the SQUID. The feedback coil is integrated in the SQUID chip, so this meant that a new SQUID with its tuned circuit had to be

prepared.

3.1 The input circuit design

The physics of a DC-SQUID like the one used in this research are outlined in my First Year Report. The input circuit is a tuned circuit which is more adequate for our purposes due to the small size of our signals. The tuned circuit has a narrower bandwidth than the untuned circuit and rings down for a while after a transmitter pulse, but it has an extra amplification factor of $\sqrt{Q}$ and is not affected by the noise outside of its narrow bandwidth. Our circuit is tuned around 1 MHz.

Figure 1 shows a diagram of the NMR circuit working in flux-locked loop (FLL).

We used a dummy set of copper receiver-transmitter coils to test the SQUID out of the cryostat. The inductance of this set was L_p=35.9μH. The capacitance consisted of two surface-mount 1206 capacitors in parallel to give a total value of 575 pF. The input coil was a 20 turns solenoid divided in two equal layers of 106 μm diameter Formvar CuNi clad NbTi. The measured inductance was 4.5 μH. The Q-spoiler consists of a number of SQUIDs connected in series. After a transmitter pulse, if the current in the input circuit is higher than the critical current of the SQUIDs in the Q-spoiler, it will drive them normal and they will become resistive. This has two advantages: first, the ring-down time is reduced, since there is not such a big current through the circuit, and second, the SQUID is protected from large flux signals ($\sim 10^6\phi_0$) coupled to the receiver coil. When operating the system in FLL, the signal from the feedback coil not only couples to the SQUID, as desired, but also couples to the input coil, generating an additional current in the flux transformer. This has an undesired effect in

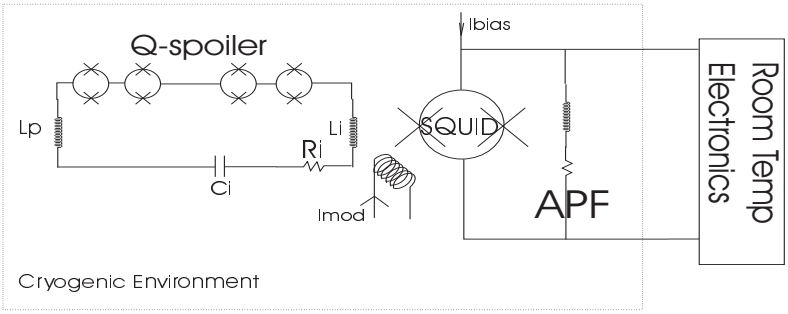

Figure 1: NMR circuit

the performance of the system. A compensation transformer consisting of a double loop of twisted wires (from the same material as the input coil) was introduced to compensate that effect. With a compensation transformer in the input circuit, therefore, the Q should be independent of the feedback resistors used. The aim was, then, to connect the transformer the right way around (by observing Q stability) and to make an estimation of the noise temperature of the system.

3.1.1 A few words about the noise temperature

The noise temperature is defined as the temperature of the resistor at which its Johnson noise is equal to the noise from the preamplifier. Below the noise temperature, then, we are limited by the noise in the preamplifier and we cannot reduce the noise by further cooling. It is desired, therefore, a noise temperature as low as possible.

Let us regard for a moment the circuit in Figure 1. If a current noise circulates in the SQUID, we have that

$$\phi_N = I_N L_s \tag{30}$$

And we can write, for the total flux in the SQUID,

$$\phi_T = \phi_N + M_i I_i = \phi_N + M_i\Big(\frac{V_i - j\omega M_i I_N}{Z_i}\Big) \tag{31}$$

Let us define

$$\omega_0 = \sqrt{\frac{1}{C_i(L_p + L_i)}} \tag{32}$$

$$Q = \frac{\omega_0(L_p + L_i)}{R_i} = \frac{1}{R_i}\sqrt{\frac{(L_p + L_i)}{C_i}} \tag{33}$$

$$\alpha^2 = \frac{M_i^2}{L_i L_p} \tag{34}$$

and

$$\alpha_{eff}^2 = \frac{M_i^2}{(L_p + L_i)L_s} = \alpha^2\Big(\frac{L_i}{L_p + L_i}\Big) \tag{35}$$

We separate now the total flux into the signal flux and the effective noise flux:

$$\phi_s = \frac{M_i}{V_i} \quad \text{and} \quad \phi_{N,eff} = \phi_N\Big(1 - \frac{j\omega M_i^2}{Z_i L_s}\Big) \tag{36}$$

We will now compare the effective noise flux with the noise at the resistor. A resistor R_i at temperature T generates a noise current

$$< I_N^2 >= \frac{4k_B T}{R_i} \tag{37}$$

which gives the voltage noise power $\frac{4k_B T}{R_i} M_i^2 V_\phi^2$ Applying the definition of noise temperature, we can now finally obtain an expression for it:

$$T_N = \Big(\frac{R_i}{4k_B M_i^2}\Big)\Big(1 + \frac{\omega_0^2 M_i^4}{R_i^2 L_s^2}\Big) < \phi_N^2 > \tag{38}$$

if we minimize T_N with respect to $\frac{\omega_0 M_i^2}{R_i L_s} = x$, we find that the optimum resistance is $(R_i)_{opt} = \frac{\omega_0 M_i^2}{L_s}$ We will now introduce the effect of the preamplifier in the expression of the noise temperature. It can be shown that then

$$T_N = \frac{(T_N)_{opt}}{2}\Big[\frac{K}{x} + x\Big] \tag{39}$$

where

$$K = 1 + \frac{< V_{N,amp}^2 >}{V_\phi^2 < \phi_N^2 >} + \frac{< I_{N,amp}^2 >}{< \phi_N^2 >}\Big(\frac{\partial \phi}{\partial I_b}\Big)^2 \tag{40}$$

and I_b is the current bias.

A final adjustment needs to be done to explain the presence of another spurious noise source. This can be parameterized by an effective resistance

in the input circuit with an effective temperature T_{eff}. And we have, finally,

$$T_N = \frac{T_{eff} R_i^*}{(R_i + R_i^*)} + \frac{(T_N)_{opt}}{2}\Big[\frac{K}{x} + x\Big] \tag{41}$$

Back to the measurements, we first identified the correct way around for the compensation transformer. The following table shows some numbers for the circuit *without* Q-spoiler and *without* compensation transformer and with different sets of feedback resistors in the read-out electronics.

Feedback Resistor	Q	Noise at Peak $(\mu\phi_0/\sqrt{Hz})$	Noise at 100 KHz $(\mu\phi_0/\sqrt{Hz})$
$2 \times 1k\Omega$	81.59	12.072	2.325
$2 \times 2.2k\Omega$	91.45	18.000	2.372
$2 \times 4.7k\Omega$	85.89	10.850	1.872
Open Loop (Shallow side)	76.29	12.396	6.898
Open Loop (Steep side)	-	9.597	1.970

It is clear that the Q depends on feedback resistors. The noise at the peak varies also within a wide range. We show now the results when a compensation transformer is attached

We see now that the Q is more stable apart from the 4.7 $k\Omega$ feedback resistors and the shallow side the open loop. But the 4.7 $k\Omega$ feedback

Feedback Resistor	Q	Noise at Peak ($\mu\phi_0/\sqrt{Hz}$)	Noise at 100 KHz ($\mu\phi_0/\sqrt{Hz}$)
$2 \times 1k\Omega$	79.30	11.65	2.213
$2 \times 2.2k\Omega$	75.10	11.371	1.731
$2 \times 4.7k\Omega$	62.27	8.023	1.746
Open Loop (Shallow side)	89.99	9.102	13.380
Open Loop (Steep side)	75.39	1.970	3.048

resistors are a relatively extreme value for feedback resistors and was taken only for completeness and the shallow side of the V-ϕ characteristic is not relevant since we are interested only in the FLL mode. The value of the noise at the peak in Flux-Locked Loop is also more stable. To make ourselves sure that the compensation transformer was connected in the proper way, we connected it the other way around and these were the results:

Feedback Resistor	Q
$2 \times 1k\Omega$	103.54
$2 \times 2.2k\Omega$	59.64
$2 \times 4.7k\Omega$	113.40
Open Loop (Shallow side)	63.57
Open Loop (Steep side)	81.39

Having identified the right way to connect the compensation transformer, we wanted to know the response of the circuit with a superconducting receiver coil, thus resembling the conditions to meet later in the cryostat. The receiver-transmitter set was removed and substituted by a superconducting receiver coil made from 90 μm diameter CuNi clad NbTi. It consisted of 46 turns of wire over 4 mm. At this point the Q-spoiler was added to the circuit. We were now in a situation of making a rough estimation of the noise temperature. The values to be used are the following:

$L_T = 16.31\mu H, \quad M_i = 3.03nH, \quad \phi_0 = 2.068 \times 10^{-15} Wb, \quad L_s = 210pH,$

$< V^2_{N,amp} >^{1/2} = 0.45nV/\sqrt{Hz}, \quad V_\phi = 412\mu V/\phi_0,$

$< \phi^2_N >^{1/2} = 1.15 \times 10^{-6}\phi_0, \quad \left(\frac{\partial \phi}{\partial I_b}\right) = 0.071 \times 10^6 \phi_0/\mu A$

and $< I^2_{N,amp} >^{1/2} = 4pA/\sqrt{Hz}$

This gives a value of 874 mK for the noise temperature, higher than the 300 mK measured inside the cryostat. But we were taking the measurements at 4.2 K, which means a higher Johnson noise from the resistive element in the circuit. Therefore, we decided to place the NMR probe in the cryostat to carry on with the superfluid experiment. Figure 2 shows the spectrum of the circuit for several feedback resistors:

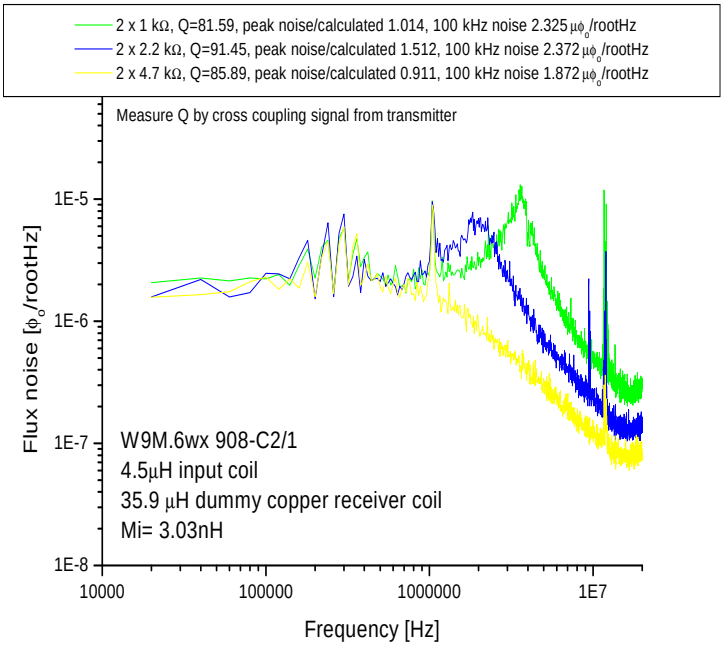

Figure 2: Noise spectrum for different feedback resistors

We can see that the noise peak does not depend on the value of the feedback resistor, which is a consequence of using a compensation transformer. We also can appreciate a reduction in the bandwidth as a function of feedback

resistors as expected. Unfortunately, once the probe went into the cryostat, there were some problems with the bandwidth and, finally, the SQUID showed a critical current which was half the value expected. Since this was noticed at helium temperatures, it was decided to continue with the experiment by running the torsional oscillator.

4 The Torsional Oscillator

A new cell has been made during this year to improve the torsional oscillator experiment. The cell, like the previous one, was fabricated from coin silver, which is supposed to have a better temperature dependent background than the usual BeCu. The head of the oscillator was linked to a coin silver body by a coin silver tube which acted as a torsion rod and fill line at the same time. The cell has a surface of around 1 cm^2. In the previous cell, the film was decoupling from the oscillator at temperatures as high as 50 mK for films as thin as 140 nm. For this experiment, the thickness of the film is always smaller than the viscous penetration depth and the inelastic mean free path at all temperatures. That means that the entire film behaves as a surface boundary layer or, in other words, the film should remain coupled to the oscillator provided that the ^{3}He is above the transition temperature. Since this was not the case, it was decided to decorate the surface of the new cell with silver particles of an average size of 600 nm diameter to "pin" the fluid. In order to do this, we made a solution of silver in ethanol with the desired amount of powder (5 mg.) and placed the cell in a teflon holder which could sustain the solution on the cell plate. The holder was left inside an ultrasonic bath overnight to get uniform spacing of the silver particles. When the ethanol was already evaporated, the cell (without the teflon) was introduced into a furnace and taken to 1000 C^o. The next step was bonding

both surfaces, top and bottom, by means of a diffusion bond. A 50 μm copper gasket ring was placed between both surfaces and a pressure was exerted. The oscillator was then taken to 750 C^o and left overnight. Before mounting the oscillator on the nuclear stage of the cryostat the cell was leak tested.

4.1 Running the Oscillator

4.1.1 System configuration and the theory underneath

The oscillator is attached to a vibration isolator block which damps the low frequency noise coming from the environment and has several different modes of resonance: floppy mode, symmetric and antisymmetric torsional modes, mainly. We operate the system in the antisymmetric torsional mode. The device is driven by a periodical force through a capacitive structure and its response is measured in the same way. The drive circuit is shown in Figure 3

The values measured for the oscillator's capacitances are $C_{1-2} = 2.89$ pF, $C_{2-3} = 4.75$ pF and $C_{1-3} = 0.04$ pF at room temperature, values that hardly changed down to liquid helium temperatures. The energy stored by a parallel plate capacitor is given by $E = 1/2CV^2$, where C is the capacitance and V the difference in potential between the plates. The capacitance is given by $C = \frac{\varepsilon_o A}{d}$ where ε_o is the specific inductive capacity of the free space, A is the surface area of the plates and d is the distance between the plates. The force exerted by the capacitor on the plates is found by taking the derivative of the energy,

$$F = -\frac{dE}{dd} = -\frac{d}{dd}\Big(\frac{1}{2}\frac{\varepsilon_o A V^2}{d}\Big) = \frac{\varepsilon_o A V^2}{2d^2} = \frac{CV^2}{2d} \tag{42}$$

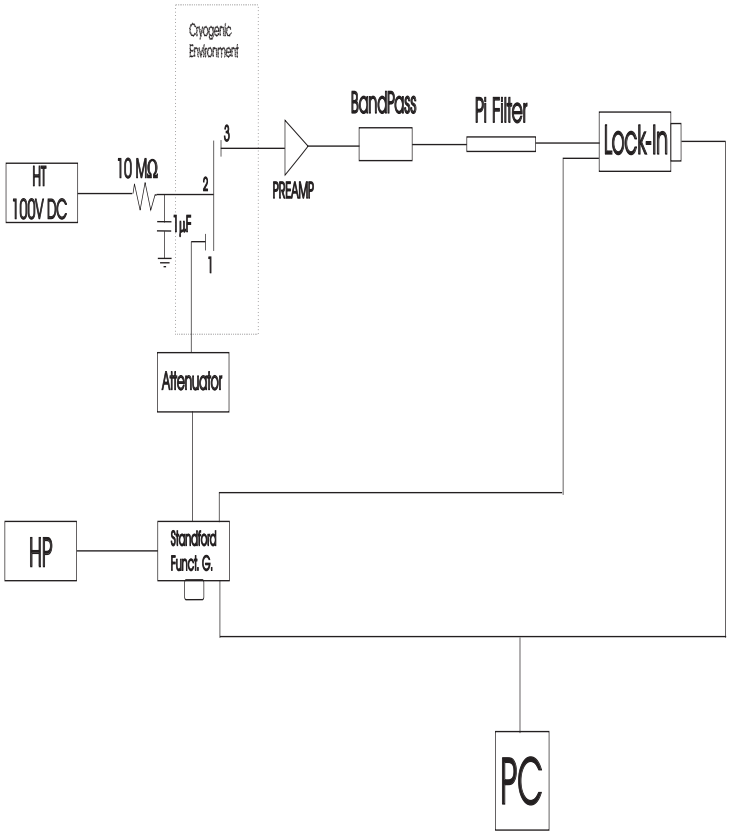

Figure 3: Experiment Setup

Clearly, this force is not linear in the voltage and this makes necessary to introduce a DC bias. Thus, with the AC excitation on top of the DC bias, we get $V = (V_o + \delta V)$ and $V^2 = (V_o + \delta V)^2 = V_o^2 + 2V_o\delta V + \delta V^2 \simeq$
$\simeq$ const. + const'.δV

δV is usually of the order of the mV and V_o uses to be chosen between 50 and 300 V. The observed amplitude is proportional to the square of the capacitance, so we choose the detector to be the higher capacitance wing in order to get maximum sensitivity.

The first stage of the experiment is to know the behavior of the unloaded oscillator as a function of the temperature. This background will be later subtracted from the film data. Past experiments with similar oscillators have shown variations in the resonance frequency at different temperatures as big as 3.5 mHz. The reason for this is not well understood yet.

Once the oscillator is mounted on the nuclear stage of the fridge, the first thing to do is to identify the antisymmetric resonance frequency. With this information we will be able at lower temperatures to excite the oscillator within a smaller frequency span, getting therefore more accurate data. To understand the way the measurements are taken we need a brief introduction to the physics of the damped and forced harmonic oscillator.

The equation of motion of a one-dimensional forced an damped harmonic oscillator is given by

$$m\frac{d^2x}{dt^2} + C\frac{dx}{dt} + Kx = F(t) \tag{43}$$

assuming that the damping is proportional to the speed. m is the oscillating mass, C and K are constants and F(t) is a periodical force which we will assume is oscillating. We will write the driving force as $F(t) = F_o e^{-i\Delta} e^{i\omega t} =$

$\widehat{F}e^{i\omega t}$ where ω is the driving frequency and Δ an arbitrary phase.

In the same way, $x(t) = 4\widehat{x}e^{i\omega t}$ (after the transient, the oscillator will resonate at the same frequency as F). Let us define $\gamma \equiv C/m$ and $\omega_o = \sqrt{K/m}$. Then, our complex equation of motion becomes

$$\frac{d^2x}{dt^2} + \gamma\frac{dx}{dt} + \omega_o^2 x = F(t)/m \tag{44}$$

Taking derivatives,

$$[(i\omega)^2\widehat{x} + \gamma(i\omega)\widehat{x} + \omega_o^2\widehat{x}]e^{i\omega t} = (\widehat{F}/m)e^{i\omega t} \tag{45}$$

And then,

$$\widehat{x} = \frac{\widehat{F}}{m(\omega_o^2 - \omega^2 + i\gamma\omega)} \tag{46}$$

Now, to separate real and imaginary part, we multiply and divide by the conjugate of the denominator:

$$\widehat{x} = \frac{\widehat{F}(\omega_o^2 - \omega^2 - i\gamma\omega)}{m((\omega_o^2 - \omega^2)^2 + \gamma^2\omega^2)} \tag{47}$$

Thus

$$Re \quad \widehat{x} = \frac{\widehat{F}(\omega_o^2 - \omega^2)}{m((\omega_o^2 - \omega^2)^2 + \gamma^2\omega^2)} \tag{48}$$

$$Im \quad \widehat{x} = \frac{-\widehat{F}\gamma\omega}{m((\omega_o^2 - \omega^2)^2 + \gamma^2\omega^2)} \tag{49}$$

If we plot $Re \quad \widehat{x}$ and $Im \quad \widehat{x}$ vs. ω, we obtain the curves shown in Figure 4

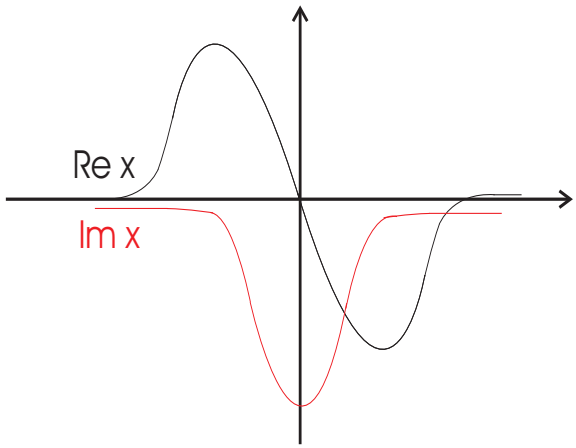

Figure 4: In-phase and quadrature components

And the energy goes as the square of the amplitude, i. e. $\rho^2(\omega) = Re^2 \quad \widehat{x}(\omega) + Im^2 \quad \widehat{x}(\omega)$

$$\rho^2(\omega) = \frac{\widehat{F}^2}{m^2((\omega_o^2 - \omega^2)^2 + \gamma^2\omega^2)} \tag{50}$$

Now, near the resonance, and for small γ ($\gamma \ll \omega_o$), $\omega \sim \omega_o$ and $(\omega_o^2 - \omega^2) = (\omega_o + \omega)(\omega_o - \omega) \simeq 2\omega_o(\omega_o - \omega)$ and $\gamma\omega \sim \gamma\omega_o$

So

$$\rho^2(\omega) = \frac{\widehat{F}^2}{m^2(4\omega_o^2(\omega_o - \omega)^2 + \gamma^2\omega^2)} \tag{51}$$

near resonance.

When the energy is half its maximum,

$$\rho^2(\omega_H) = \frac{1}{4\omega_o^2(\omega_o - \omega_H)^2 + \gamma^2\omega^2)} \tag{52}$$

and

$$\begin{aligned} 4\omega_o^2(\omega_o - \omega_H)^2 + \gamma^2\omega^2 &= 2\gamma^2\omega_o^2 \\ 4(\omega_o - \omega_H)^2 &= \gamma^2 \\ (\omega_o - \omega_H)^2 &= \gamma^2/4 \\ \omega_o - \omega_H &= \pm\gamma/2 \\ \omega_H &= \omega_o \pm \gamma/2 \end{aligned}$$

So γ means the width at half height for the energy.

A very important quantity is Q, the quality factor, which is defined as $Q = \omega_o/\gamma$. The physical meaning of Q is the energy stored per cycle over the

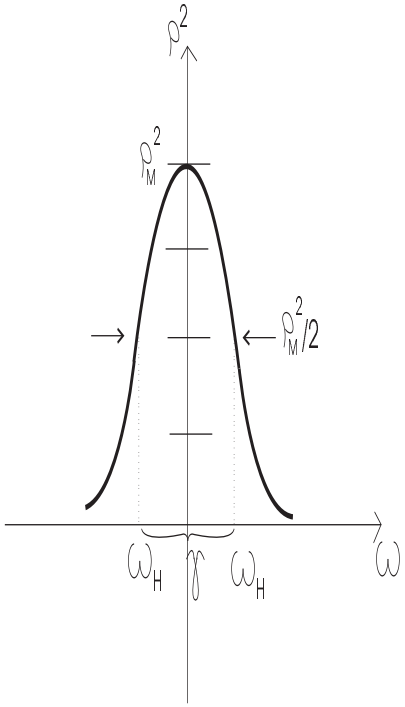

Figure 5: Energy Vs. Frequency

power loss. In our experiment, we use to get the factor γ from the amplitude rather than from the square of the amplitude. The only difference is that we then evaluate $\rho(\omega)$ at $\rho_{max}/\sqrt{2}$ to get the width in frequencies.
Since we are dealing with a torsional pendulum, and not with an oscillating mass, the factor m in the equations above should be replaced by I, the momentum of inertia of the oscillator.

4.1.2 Setting up the experiment

Room temperature.

We drive our empty cell within a range of frequencies from 2000 Hz to 3000 Hz to find the antisymmetric torsional mode. This is done first out of the cryostat, in a vacuum can. Once found the resonance, the oscillator is mounted on the nuclear stage of the cryostat and finer sweeps are done.
The Lock-In Amplifier records the imaginary part of the resonance in the X channel and the real part in the Y channel. The resonance frequency at room temperature was found to be around 2448 Hz. The next sweep was set to be from 2448.5 Hz to 2450.8 Hz. DC bias here was 50 V. Points were measured every 5 mHz and the drive voltage was 400 mV p-p. The holding time was 12 seconds. This parameter, the holding time, is important because if it would be too short, we would pick some ring-down. In other words, we have to let the transient solution of the equation of motion stated above to vanish. From the definition of Q, $Q = \omega_o/\gamma$, and the transient goes as $e^{-\gamma t/2}$ (solving homogeneus equation of motion). So the decay time would be given by $\gamma\tau/2 = 1$ (this is the time at which the resonance would be reduced by a factor 1/e).
So $Q = \frac{\omega_o \tau}{2} = \pi f_o \tau \rightarrow \tau = \frac{Q}{\pi f_o}$
At room temperature, $Q \sim 10^4$, $f_o \sim 2 \times 10^3$ and $\tau \sim \frac{10^4}{\pi 2 \times 10^3} \sim 1.6s$

This time will need to be much longer at lower temperatures. We can see the resonance at room temperature in Figure 6.

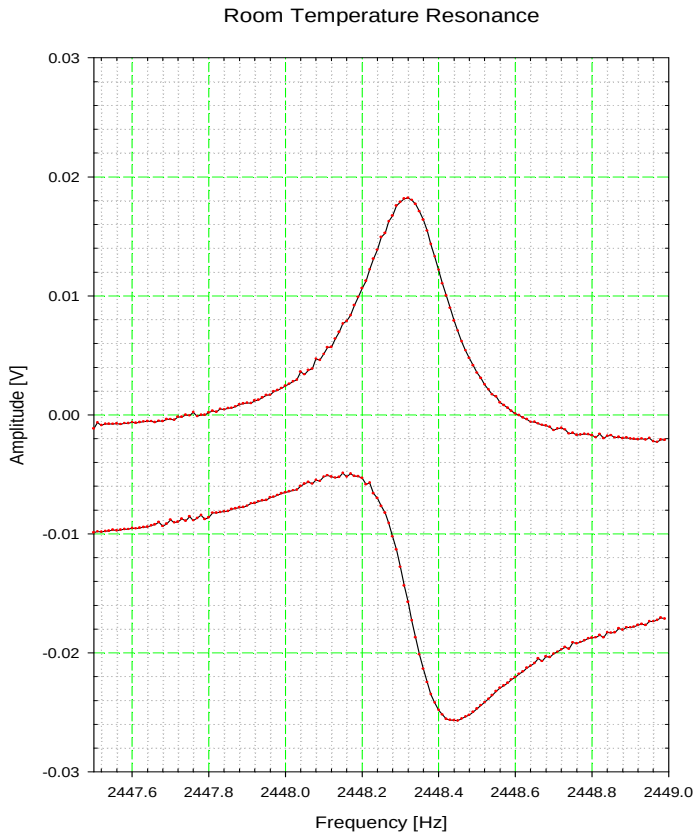

Figure 6: Room Temperature Resonance

We can see that the plot differs from the theoretical introduction by a phase of 180 degrees, that is, we keep the imaginary part positive. This has no effect on the amplitude of the pendulum neither on the Q or the resonance frequency. That only affects the setting of the phase in the

Lock-In amplifier. We will deal with that problem later.

It is evident from the plot that the phase is not zero at resonance (from now on we will understand by phase Arc Tg (Y/X), regarding X as positive. That implies that the phase at resonance is zero, whereas with the theory introduced above the phase at resonance is 180 degrees). The maximum amplitude, the Q and the resonance frequency where obtained by fitting the X component to a Lorentzian. This method is not correct, since the Q is defined with respect to the amplitude, but is enough to get a "feeling" for the numbers. At lower temperatures, another method was used.

Liquid Nitrogen temperature.

Everything said for the room temperature case can be repeated here. We can see that the resonance frequency has shifted to a higher value. Q is also larger. The maximum amplitude has decreased and the phase is still wrong. Regarding the holding time, now $Q \sim 5 \times 10^4$, so $\tau \sim 8$ sec. The current holding time (12 seconds) is therefore still valid. The X and Y channels at liquid nitrogen temperatures are shown in Figure 7.

Liquid Helium temperature.

In this measurement it could be that the holding time is not long enough. $Q \sim 8 \times 10^4 \rightarrow \tau \sim 13$ sec. f_o and Q keep increasing with lower temperatures. The phase needs to be corrected in the Lock-In amplifier in order to obtain zero at resonance. With a zero-phase resonance we could then fit a Lorentzian to the *amplitude* of the resonance without manually treating the data and get a valid number for the Q. The actual value of Q needs to be known accurately at some given temperature in order to infer the resonance frequency at much lower temperatures. Figure 8 shows the resonance.

60 mK.

With the nuclear stage stabilized at 60 mK, the oscillator was driven this

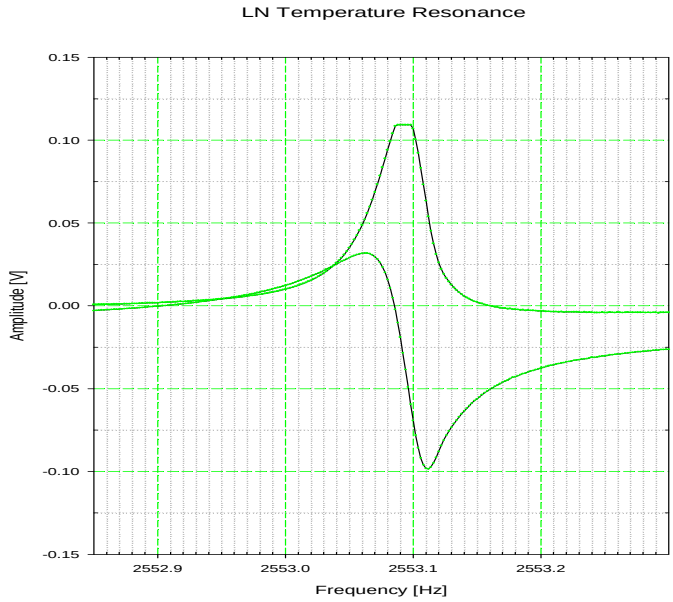

Figure 7: Liquid Nitrogen Resonance

time through the attenuator with an amplitude of 10x0.2 mV p-p. The holding time was now 1 minute (expected to be enough $Q \sim 3 \times 10^5 \rightarrow \tau \sim$ 5 sec.) The resonance can be seen in Figure 9.

At this point, the 10 MHz output of HP was connected to the Stanford generator to improve the Stanford internal clock. The feedthrough was observed to be in both, X and Y channels, about 0.2 mK, more or less 10 times worse than in previous oscillators. DC bias was then increased to 100 V to make sure that we were working in the linear regime. Also, the HT output was not properly connected and it was changed to the diagram shown in Figure 3. After this sweep, an offset of 2.5 V was found on the output of the Stanford which affected the drive. It was removed and the

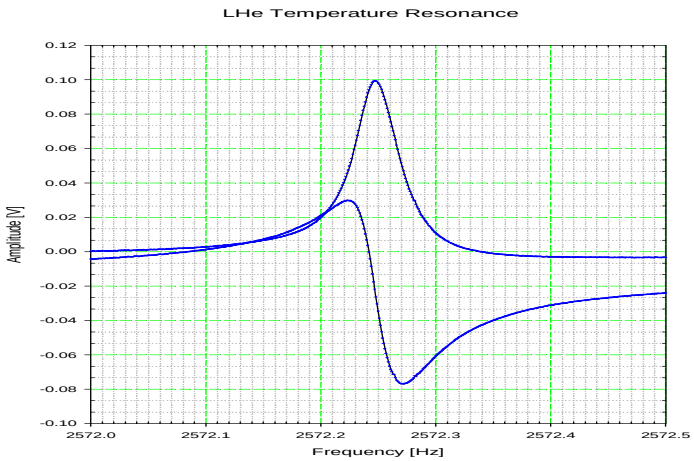

Figure 8: Liquid Helium Resonance

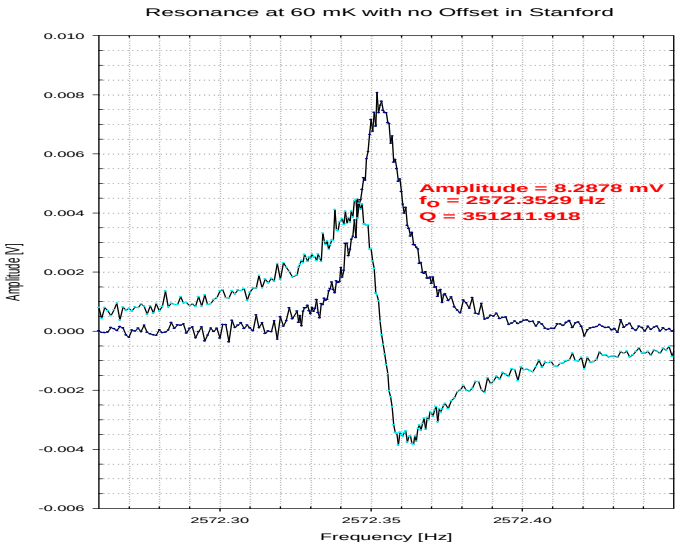

Figure 9: Resonance at 60 mK

output was taken through the 2→4 KHz badpass filter.

In order to get the phase in the Lock-In right, we firs measure the

feedthrough by switching off the DC bias ($X = -7.988 \times 10^{-6}V$; $Y = -2.1147 \times 10^{-5}V$). These values are going to be subtracted from the data in the next measurements. We now take the X and Y subtracted data and plot the amplitude vs. frequency and fit it to a Lorentzian. We thus get a resonance frequency. The next step is to plot the phase (Arc Tg(Y/X)) vs. (frequency-resonance frequency). A linear fit near zero of the last plot will give us the phase at resonance. That number is added to the phase on the Lock-In to achieve zero phase at resonance. The Lock-In final value for the phase was $+179.40^o$

Inferring the resonant frequency at a constant drive

When running the experiment it would be impossible to make a sweep for each temperature studied. The solution is to infer the resonance frequency from the measured values of X and Y in the Lock-In. The method is as follows. The ratio Q/A in the oscillator, being A the amplitude on resonance, is a constant proportional to the driving force. It is clear, then, that if we know the Q and the amplitude at some temperature, we can know the Q at any other by just measure the amplitude on resonance. We have

$\frac{Y}{X} = \frac{\omega_o^2 - \omega^2}{\gamma\omega}$ with our new definition of positive X. Now some easy algebra, $\gamma = \omega_o/Q$ from the definition of Q. Thus, $\frac{Y}{X} = \frac{Q\omega_o^2 - \omega^2}{\omega_o\omega}$

$$XQ\omega_o^2 - Y\omega\omega_o - XQ\omega^2 = 0$$

$$\omega_o = \frac{Y\omega \pm \sqrt{Y^2\omega^2 + 4X^2Q^2\omega^2}}{2XQ}$$

The minus sign has no physical meaning ($\omega > 0$)

$\omega_o = \frac{Y\omega}{2XQ} + \sqrt{\frac{Y^2\omega^2}{4X^2Q^2} + \omega^2} =$

$= \frac{Y\omega}{2XQ} + \omega\sqrt{1 + \frac{Y^2}{4X^2Q^2}}$

Now, near resonance, $Y^2/X^2 \ll 1$ and $\sqrt{1+X^2} \to (1 + X^2/2)$

$\omega_o = Y\omega/2XQ + \omega(1 + Y^2/8X^2Q^2) =$

$= \omega(1 + \frac{Y}{2XQ} + \frac{Y^2}{8X^2Q^2}) \simeq \omega(1 + \frac{Y}{2XQ})$

We call $\omega \equiv f_D$ (Driving Frequency) and $\omega_o \equiv fI$ (Inferred Frequency)

Let us calculate how can we deduce Q by knowing X and Y. We know that $Q/X_{MAX}(T_1) = Q/X_{MAX}(T_2)$. Therefore we only need to know X_{MAX} to deduce Q. How to know X_{MAX} from X and Y?

If we plot the Nyquist circle,
The diameter is X_{MAX}. Then, after Pythagoras:

$$2R = X_{MAX}$$
$$X'^2 + Y^2 = R^2$$
$$X' = R - X \Rightarrow R = \frac{X^2 + Y^2}{2X}$$

Then $X_{MAX} = 2R = \frac{X^2+Y^2}{X}$. Now, $Q = (q/a)X_{MAX} = (q/a)\frac{X^2+Y^2}{X}$ where q and a are the values of Q and X_{MAX} at some temperature. We have therefore a routine to infer the frequency when driving the oscillator at a

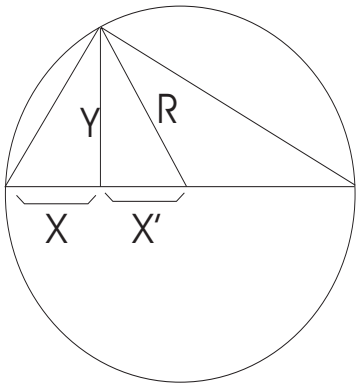

Figure 10: Nyquist circle

fixed frequency near the resonance frequency:

$$f_I = f_D\Big(1 + \frac{Ya}{2q(X^2+Y^2)}\Big) \tag{53}$$

We made a very careful sweep at 60 mK and we got $Q = 193409.88$ and $A = 9.65mV$. These are the numbers used to infer the resonance frequency throughout the experiment.

4.1.3 Results

First of all, we need to know the behavior of the empty cell. To get this background, the temperature is changed in small steps within the range of interest (150 mK to base) and we wait at each step for some time (of the order of hours) to let the oscillator to stabilize. Once the frequency is stable, the oscillator is retuned and the value of the inferred frequency is averaged over few minutes. The background measured is shown in Figure 11.
Two curves are calculated to fit the data, one from base (0.3 mK) to 25 mK and the other from 25 mK to 150 mK. With this information we can no proceed to fill the cell. The filling procedure was not as fine as desired due to constant jumps in the oscillator's resonance. In order to fill the cell, the temperature was set to be 60 mK and the filling line was heated as the ^{3}He was released into it from the room temperature gas handing system. The temperature was then taken to 490 mK where the gas slowly entered the cell. The frequency shift was measured and that gave us a guess on the film thickness. For the oscillator, $\Delta f = \frac{\Delta I}{2I} f_o$ where I is the momentum of inertia of the whole system (oscillator plus sample). A $1000\mathring{A}$ thick ^{3}He film has a momentum of inertia $(\Delta I)_{1000\mathring{A}} = 1/2\rho h\pi R^4 = 3.09 \times 10^{-7} g cm^2$, being $R = \quad 0.7cm$ the radius of the disc, $\rho = 0.082 \quad g/cm^3$ the density of

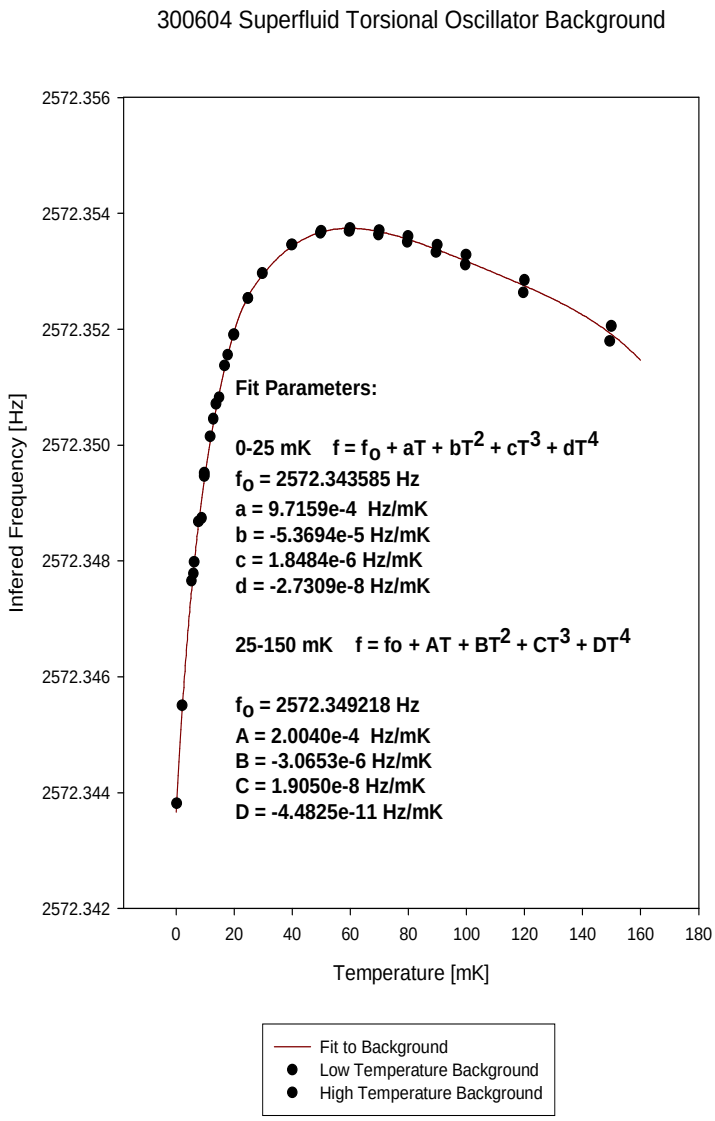

Figure 11: Empty cell temperature dependence

^{3}He at zero temperature and h the thickness of the film. The momentum of inertia of the cell is $I = 0.875gcm^2$ and the resonance frequency is $f_o \sim 2.5kHz$. All this gives a value of $\Delta f = 0.909mHz/1000\mathring{A}$. This estimate is, nevertheless, very rough, since during the process of filling, any event in the cryostat or surroundings (changes in pressure in the recovery line due to other helium transfers, etc...) was critical to the inferred frequency. The optimum measurement would be to measure the resonance frequency at 60 mK and then, after filling the cell at 490 mK, back to 60 mK, to measure the total shift. In our case, the shift, as said, was continuously monitored at 490 mK.

We have measured three samples. The first one from a 0.92 mHz shift ($1012\mathring{A}$ thickness), the second from 2.75 mHz ($3025\mathring{A}$ thickness) and the third from 1.65 mHz shift ($1815\mathring{A}$ thick film).We observed interesting features in all of them. For the first coverage, we show the low temperature behavior in Figure 12.

We can see a sudden change in slope on warming. This happens around the bulk ^{3}He superfluid transition. But, surprisingly, the change is from *high* to *low* momentum of inertia, which is the opposite one could expect. As the superfluid couples back to the oscillator, the momentum of inertia should increase. This is not well understood yet, although one possible explanation could be a redistribution of the fluid within the cell as the transition occurs. The second coverage was much thicker and the results were astonishing at first sight. They are plotted in Figure 13.

The figure shows the inferred frequency in cooling and warming as well as the dissipation (1/Q) vs. time. The most remarkable characteristic is the symmetry of the plot. The events on cooling were exactly (apart from some disturbances due to helium transfers into the fridge) reproduced. There is

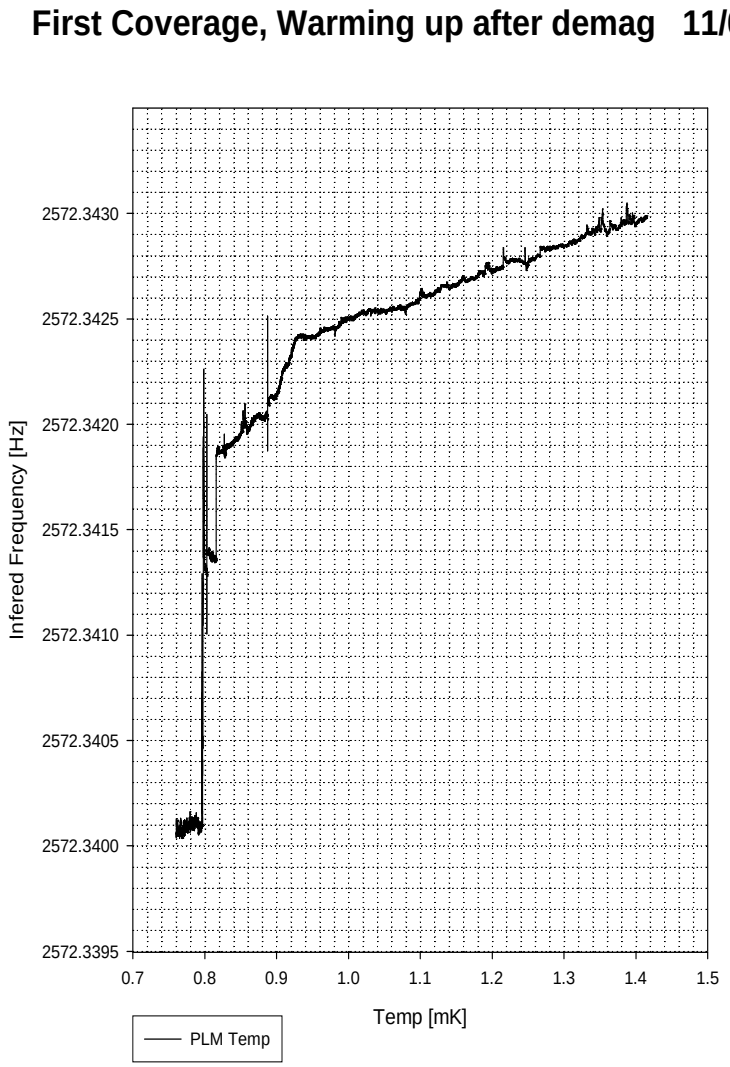

Figure 12: Low temperature Data for First Coverage

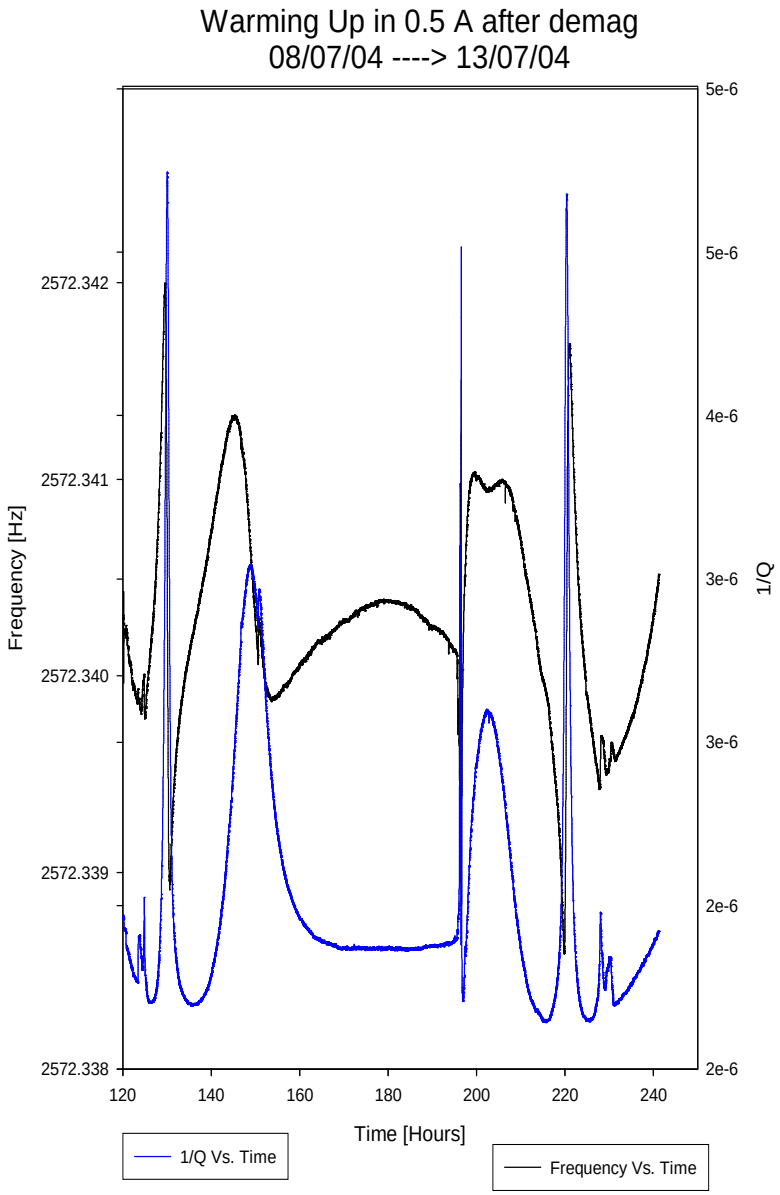

Figure 13: Low temperature Data for Second Coverage

also a sharp peak whose magnitude is comparable to the total load of the cell. All this mounts and valleys could be interpreted as transitions but there is a subtle characteristic which tells us otherwise. If we look the dissipation for a moment, we see that the dissipation and the frequency resemble the in-phase and quadrature components of a resonance! There are two of them and they could be attributed to some sound in the fluid coupled to the oscillator. There are five main sounds in ^{3}He. The first sound is similar to the ordinary sound, that is, pressure waves with changes in density. The second sound is a mode in which the superfluid and the normal components of the sample move out of phase and there are not pressure gradients. There is an oscillation in the local entropy, a heat wave, and is propagated by phonons. Third sound is related to waves in the surface of a thin film of superfluid and the normal component takes no place on it. Fourth sound, like third, is only related to the superfluid part of the liquid, and the normal fluid remains clamped. It occurs in restricted geometries where the normal component is locked to the walls due to its viscosity while the superfluid is free to flow. Finally, there is a final mode, the zero sound, first suggested by Landau, and which is the only one taking place in the collisionless limit ($\omega\tau \gg 1$ with τ being the mean quasiparticle collision time). First and Second sound are discarded for our experiment, since they involve motion of the normal fluid. Third sound could be a candidate, but the frequency of third sound is of the order of Hertzs, and we are working in kHz. Zero sound, on the other hand, takes place a frequencies as high as megaHertzs. The remaining candidate is fourth sound and that is the mode we believe is coupled to the oscillator. That would mean that there is a superfluid transition *different* than that of bulk inside the cell. The velocity of fourth sound $c_4 \propto \sqrt{\frac{<\rho_s>}{\rho}C_1}$ which means that fourth sound is for the superfluid the equivalent of first sound for

the normal liquid. If that would be our case, this could be used to measure the fraction of superfluid in the sample. This film was demagnetized twice in order to check reproducibility and the behavior was, basically, the same. A third sample was studied as shown in Figure 14.

This was a film of an intermedius thickness compared with the previous two. Here there is, finally, a shift which agrees with our expectancies. The film begins to decouple at some point between one mK and half a mK. The measurement of the temperature is slightly difficult, since the thermometer used for this purpose, the PLM NMR thermometer, had a different heat link to the nuclear stage from the link of the oscillator. We observed that the oscillator was briefly retarded in response with respect to the PLM thermometer. Finally, in Figure 15. we present all three coverages as a function of temperature and plotted with the extrapolation of the background.

It is remarkable the qualitative agreement of all three samples (which were all shifted by a constant frequency to match the background) with the empty cell line. Also, the fact that all the coverages show a change in behavior at the same temperature (about the bulk transition temperature) is encouraging. The three different thicknesses behave in a complete different way between each other. Only the thicker film showed what is thought to be fourth sound coupling and the other two films showed opposite trends. Comparing this results with other experiments [26] [29] we observe that both reported some remarkabilities at similar thicknesses as ours. Xu and Crooker observed a difference in the rate of transition depending whether the films were thinner or thicker than 137.5 nm (real thickness). The group of Berkeley measured a change in third sound velocity for thicknesses above 170 nm (real thickness) although they attributed that to the competition between the superfluid

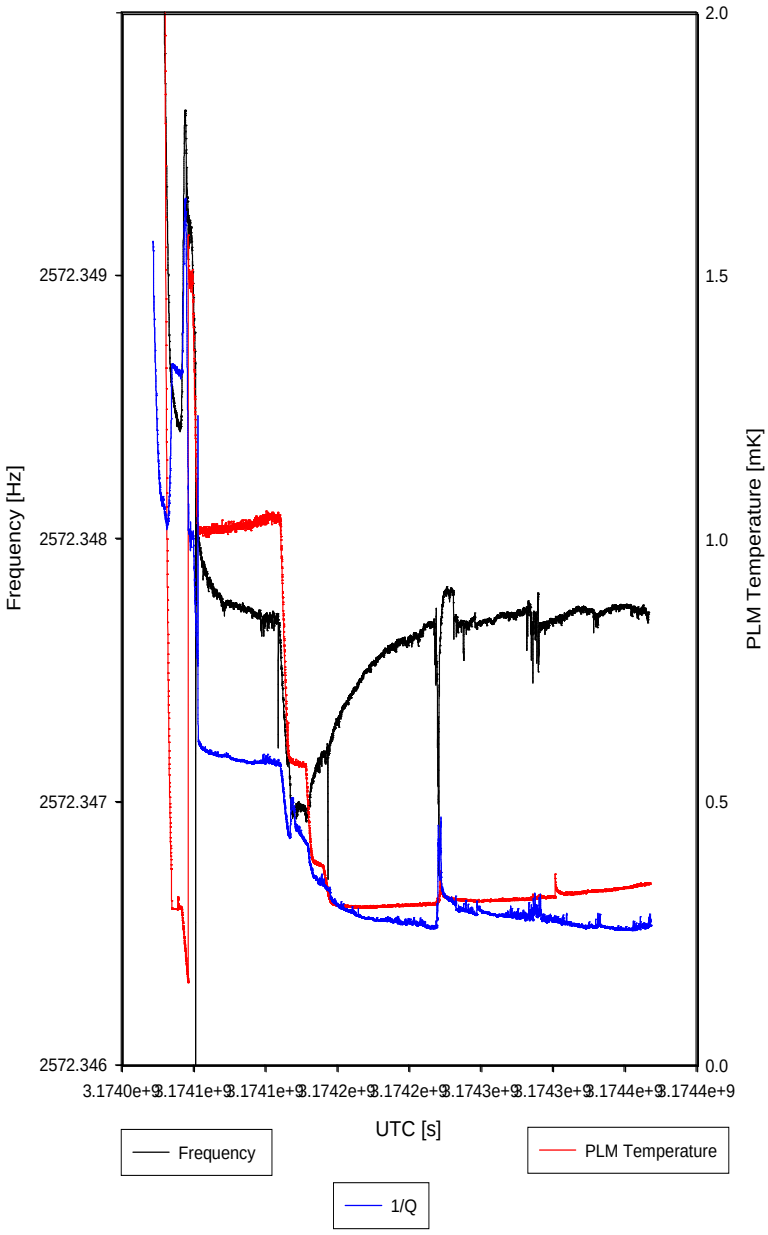

Figure 14: Low temperature Data for Third Coverage

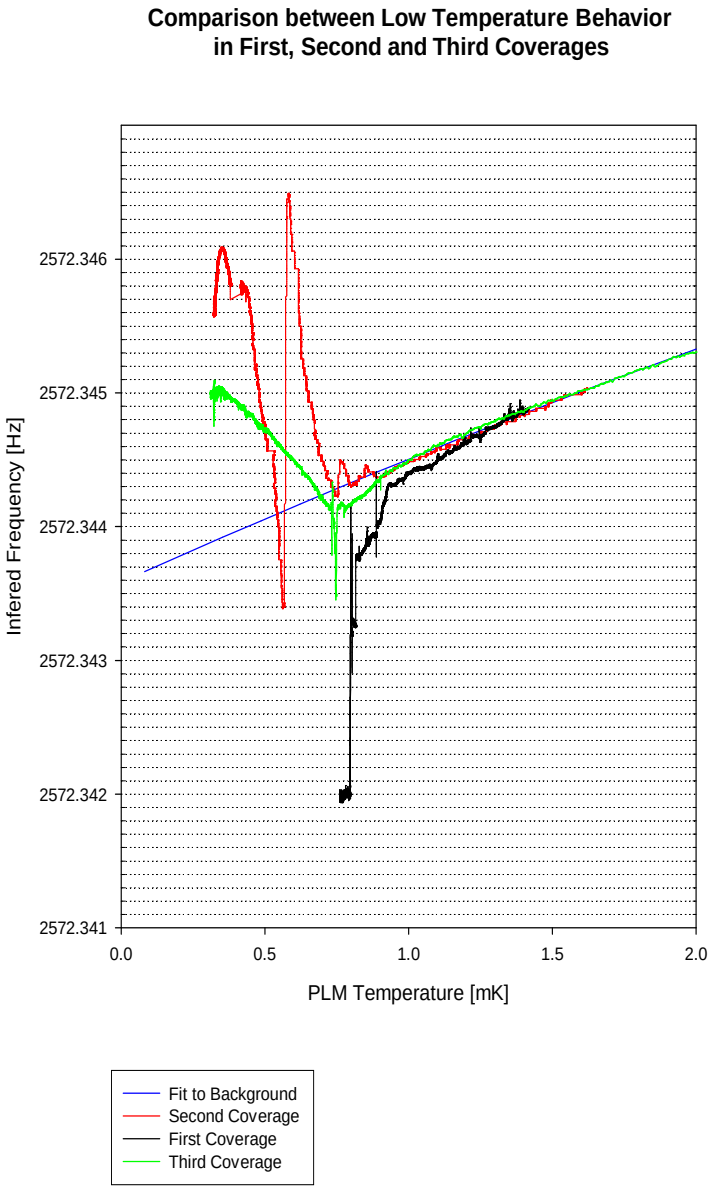

Figure 15: Samples comparison

density rising and the van der Waals force falling with the film thickness. In our experiment, we get qualitatively opposite behaviors between the 101.2 nm thick film and the 1.815 nm thick film, which lies within the same range. To further investigate this system we are at the time of writing preparing a fourth sample, aiming for a thickness between the first and the third sample (around 140 nm).

5 Additional and future work

5.1 The problem of the capillary condensation

Shortly after the obtention of our NMR data last summer, we realized that there was a major issue regarding the morphology of our sample within the disc-shaped cell. The problem was that the capillary condensation of the liquid in the corners of the cell was a real possibility. At the moment, the problem has not been satisfactorily solved, but we know that the threshold thickness for the condensation to happen is of the order of our sample's size. We received a comment from a referee regarding a prospective publication about the torsional oscillator experiment. In this comment the referee made a rough estimation of 630 nm. for the thickness at which the helium would stop joining the film and would join the meniscus instead. The idea was the following:

Beyond 40 nm. the liquid presents a semicircular profile in the corners. The surface energy per unit volume in a liquid is

$$E_S = -\gamma(\frac{1}{R} + \frac{1}{r}) \tag{54}$$

where R and r are the two principal radii of curvature(we regard R and r as positive if they are drawn into the medium with smaller pressure). γ is

called the surface tension coefficient and for ^{3}He its value is $156\mu J/m^2$. The film energy per unit volume is

$$E_F = -\frac{gd_o}{1.4d^4} \tag{55}$$

where d is the thickness of the film, g is $4.7x10{-}50Jm^3$/atom and d_o is 20 nm. E_S will change, through the parameter R, whenever we add some liquid to the meniscus. E_F, on the other hand, will change whenever we add some liquid to the film. Let us calculate the change in each of these energy densities when we add a small volume of helium to the cell.

$$\frac{dE_S}{dV} = \frac{dE_S}{dR} \cdot \frac{dR}{dV} = \Big(\frac{\gamma}{R^2}\Big)\Big(\frac{-1}{2\pi Rt}\Big) \tag{56}$$

where R is the disc space radius and t is the space height. The volume of the cell is $V = \pi R^2 t$ and the change in that volume is the change in the volume of the liquid with opposite sign. Note that the energy in the vertical direction is not supposed to change in this situation. Now, the change in the film energy density is

$$\frac{dE_F}{dd} \cdot \frac{dd}{dV} = -\frac{4gd_o}{1.4d^5} \cdot \frac{1}{2\pi R^2} \tag{57}$$

since now the volume of the film layer is $V = 2\pi R^2 d$. If we now make this two quantities equal we find a critical thickness of 630 nm. That is, for d<630 nm, the liquid would join the film and beyond that, the sample would grow from the sides, which is unwanted.

Although quite optimistic, I do not quite believe the above proposition for, mainly, two reasons. First, it is not clear to me why the energy density, rather than the energy, is used. That involves a second order derivative when

minimizing and surely affects the final number. Secondly, when we change the thickness of the film, not only d, but also r change. The change in r is quite small, but because the energy dependence goes as 1/r, this change would affect the treatment dramatically, lowering the obtained threshold by a substantial amount. That could mean that in our present geometry it is not possible to grow a stable film. The problem is still open and the measurements will, surely, have something to say about that.

5.2 What now?

One of the main projects for the incoming year is the design and development of a confined cell. This cell, as explained in my first year report, would consist of a gap of the desired film thickness (around half a micron) and would be made out of some nonmagnetic material such as glass or silicon. The glass cell would have the following characteristics: Two polished fused silica discs of 16 mm. diameter and 3 mm. thick with a flatness of approximately $\lambda/20$. Deposited fused silica annular spacer on one disc giving 10 mm. internal diameter. One venting hole of approximately 1 mm. diameter. Spacer thickness of approximately 500-1000 nm. with an error of $\pm$ 2%. Optically contacted and sealed with cement. This cell would be provided by the company *IC Optical Systems LTD* with which some contacts have been already made. The optical bonding was leak tested in two optical flats, but was found to leak at nitrogen temperatures. That means that the bonding needs to be improved. The silicon cell is a current project by a group at Cornell University in USA. The characteristics would be similar to those of the glass cell.

The main problem when designing a confined cell is to separate the filling line NMR signal from the signal of the confined liquid, because the bulk signal is

larger than the film signal and overshadows it. But making a reliable contact between metal and glass at low temperatures is not a trivial problem because of the different thermal compressibilities. A possible, although not the most desiderable, solution would be to treat the bulk signal *as a background* and subtract it from the film data. With a confined cell we would not be able to change the film thickness, of course. But the parameter we are interested in is not quite the film thickness, but the relative thickness, that is, the thickness divided by the coherence length. And we surely can vary the coherence length by changing the pressure in the cell. So the tuning method is different in different cells but it is still possible to explore the phase diagram in a similar way. A minor problem here is that the maximum in coherence length occurs at zero pressure, so in the confined cell we could only *reduce* the coherence length and, therefore, only make the film *thicker* in the sense of the current cell.

Finally, the plan for the incoming year includes the repair of the SQUID spectrometer, further investigating the problems that the SQUID circuit has at the moment, and, if possible, carry on with the NMR measurement where it was left last summer. As a part of this we will study the system with the gradient coils in the cryostat, trying to map out the morphology of the sample. Making a set of Golay coils is also an interesting possibility. The NMR experiment is TOP 1 priority at the moment, due to the promising results obtained last year and the endless problems found when trying to run it again. The Torsional Oscillator has proven also successful as a technique, so running it again during next year is not discarded. The compatibility of both, the NMR and the Torsional Oscillator tecniques makes possible the operation of the two methods at the same time. In brief, the results during my 20 months of research are nothing but encouraging and rewarding and,

albeit there is still a long way to walk, the final target of this experiment seems within arm's reach.

References

[1] J. Bardeen, L. N. Cooper, and J. R. Schrieffer, *Phys. Rev.*, Vol. 108, 1175

[2] P. W. Anderson and P. Morel, *Phys. Rev.*, Vol. 123, 1911

[3] R. Balian and N. R. Werthamer, *Phys. Rev.*, Vol. 131, 1553

[4] D. M. Lee, *Rev. Mod. Phys.*, Vol. 69, 645

[5] D. D. Osheroff, W. J. Gully, R. C. Richardson and D. M. Lee, *Phys. Rev. Letters*, Vol. 29, 920

[6] A. J. Leggett, *Rev. Mod. Phys.*, Vol. 47, 331

[7] L. D. Landau, *ZETP*, Vol. 7, 19. English translation in *Collected Papers of L. D. Landau*, D. ter Haar, e., Gordon and Breach, London, p. 193

[8] V. L. Ginzburg and L. D. Landau, *ZETP*, Vol. 20, 1064. English translation in *Collected Papers*, p. 546

[9] L. P. Gorkov and Zh. Eksperim, *Soviet Phys. JETP*, Vol. 9, 1364

[10] J. C. Wheatley, *Rev. Mod. Phys.*, Vol. 47, 415

[11] D. m. Lee and R. C. Richardson, *Superfluid ^3He*, page 287 of *The physics of liquid and solid helium, part II*, K. H. Bennemann and J. B. Ketterson, Wisley Interscience

[12] P. W. Anderson and W. F. Brinkman, *Phys. Rev. Lett.*, Vol. 30, 1108

[13] V. Ambegaokar, P. G. deGennes and D. Rainer, *Phys. Rev. A*, Vol. 9, 2676

[14] A. B. Vorontsov and J. A. Sauls,*arXiv:cond-mat/0304054*, Vol. 1, Apr 2003-08-12

[15] Z. Tešanović and O. T. Valls, *Phys. Rev. B*, Vol. 31, 1374

[16] Z. Tešanović and O. T. Valls, *Phys. Rev. B*, Vol. 33, 3139

[17] Z. Tešanović, *Phys. Lett.*, Vol. 100A, 158

[18] A. L. Fetter and S. Ullah, *JLTP*, Vol. 70, 515

[19] J. M. Kosterlitz and D. J. Thouless, *J. Phys*, Vol. 6, 1181

[20] J. Corson, R. Mallozzi, J. Orenstein, J. N. Eckstein and I. Bozovic, *Nature*, Vol. 398, 221

[21] D. L. Stein and M. C. Cross, *Phys. Rev. Lett.*, Vol. 42, 504

[22] H. C. Dyball, *Ph. D. Thesis* Royal Holloway University of London, 2001

[23] A. Sachrajda, R. F. Harris-Lowe, J. P. Harrison, R. R. Turkington and J. G. Daunt, *Phys. Rev. A.*, Vol. 7, 790

[24] J. C. Davis, A. Amar, J. P. Pekola and R. E. Packard, *Phys. Rev. Lett.*, Vol. 60, 302

[25] M. R. Freeman, R. S. Germain, E. V. Thuneberg and R. C. Thuneberg, *Phys. Rev. Lett.*, Vol. 60, 596

[26] J. Xu and B. C. Crooker, *Phys. Rev. Lett.*, Vol. 65, 3005

[27] Y. Li and T. Ho, *Phys. Rev. B.*, Vol. 38, 2362

[28] L. H. Kjäldman, J. Kurkijärvi and D. Rainer, *JLTP.*, Vol. 33, 577

[29] A. M. R. Schechter, R. W. Simmonds, R. E. Packard and J. C. Davis, *Nature*, Vol. 396, 554